Sulfur and Ti^{3+} co-Doping of TiO_2 Nanotubes Enhance Photocatalytic H_2 Evolution Without the Use of Any co-catalyst

Lei Ji,[a,b] Xuemei Zhou,[a] and Patrik Schmuki*[a,c]

[a] Prof. L. Ji, Dr. X. Zhou, Prof. P. Schmuki*
Department of Materials Science WW-4, LKO; University of Erlangen-Nuremberg, Martensstrasse 7, Erlangen 91058 (Germany). Email: schmuki@ww.uni-erlangen.de
[b] Prof. L. Ji
College of Chemistry and Chemical Engineering, Northeast Petroleum University, Provincial Key Laboratory of Oil and Gas Chemical Technology, Daqing 163318 (China)
[c] Prof. P. Schmuki*
Department of Chemistry, Faculty of Science, King Abdulaziz University, P.O. Box 80203, Jeddah 21569 (Saudi Arabia)

Link to the published article:
https://onlinelibrary.wiley.com/doi/full/10.1002/asia.201900532

Abstract: TiO_2 nanotubes were successfully co-doped with sulfur and Ti^{3+} states using a facile annealing treatment in H_2/H_2S gas mixture. The obtained nanotubes were investigated for their photocatalytic performance and characterized by SEM, XRD, XPS, EPR, IPCE, IMPS and Mott-Schottky measurements. The synthesized co-doped TiO_2 nanotubes show an enhanced photocatalytic hydrogen production rate compared to tubes that were treated only in pure H_2 or H_2S atmosphere – this without the presence of any co-catalyst. It was found that sulfur in co-doped TiO_2 exists in the form of S^{2-} and a small quantity of S^{4+}/S^{6+}, which leads to a narrowing of the band gap. However, the enhanced absorption of light in the visible range is not the key reason for the improved photocatalytic performance. We ascribe the enhanced photocatalytic activity to a synergetic effect of S mid-gap states and dislocated Ti^{3+} defects that facilitate photo generated electron transfer.

Keywords: TiO_2 nanotubes • Hydrogen evolution • Oxygen vacancy • Ti^{3+} • Sulfur doping

Introduction

Since the discovery of photocatalytic water splitting in 1972 using a titanium dioxide (TiO_2) photoanode,[1] TiO_2 has attracted wide research interest as a photocatalyst in the fields of organic pollutant degradation and photocatalytic H_2 generation.[2-4] Titanium dioxide, as a photocatalyst, provides intrinsic advantages over other photocatalysts, such as a high chemical stability, low-cost, high abundance, low toxicity and high corrosion resistance.[5-7] However, TiO_2 carries also some drawbacks that limit its efficient application. Key deficits are the relatively large optical band-gap (3.2 eV for anatase or 3.0 eV for rutile) that allows only for the use of approx. 7% of solar light, as well as the sluggish charge transfer to aqueous reactants. Accordingly, many efforts have been made to enhance the photo activity by extending the working spectrum of TiO_2 to the visible light region by band-gap engineering,[8] and to improve the kinetics of photo generated carrier transfer across the TiO_2/environment phase boundary.

For example, doping of TiO_2 with non-metal elements (such as C, N and S) has been widely explored to tune the electronic structure of TiO_2; namely to narrow the band gap for visible light response.[9-10] Chen and Burda investigated the electronic origin of the visible light absorption properties of non-metal doped TiO_2 by XPS and found that additional electronic states above valence band edge led to a red-shift of absorption.[10] Among these dopants, sulfur (S^{2-}) is regarded as a promising candidate not only because of suitable energetics but also because it has the same valence as oxygen and hence does not introduce a charge imbalance. Since then, several groups have reported on the beneficial effect of S-doping of TiO_2 for an enhanced photocatalytic activity under visible or UV light.[11-15] Tang *et al*.[16] reported that sulfur-doped TiO_2 nanotubes could be prepared by annealing TiO_2 in a flow of H_2S leading to incorporation of S^{2-} into the oxygen sites of TiO_2 and formation of O-Ti-S bonds. However, Shin *et al.* reported sulfur in the form of both Ti-S and sulfate, as detected for S-doped TiO_2 nanotube arrays after annealing at high temperature in N_2/H_2S mixture gas.[15]

More recently, self-doping of TiO_2 by introducing intrinsic Ti^{3+} defects was discussed as a new approach, where the defects can narrow the band gap of TiO_2 (this process usually leads to black or other dark colors).[3,17-18] In order to establish suitable Ti^{3+} states, a variety of synthetic approaches have been explored,[19-24] among them hydrogenation of crystalline TiO_2 to "grey TiO_2" that can provide considerable activity for photocatalytic hydrogen production in absence of a noble metal co-catalyst.

Considering above, one may rationalize that both S-doping of TiO_2 (extending the absorption wavelength region) and establishing desired Ti^{3+} centers can in principle be achieved by a suitable heat treatment of TiO_2 in H_2/H_2S environments. Herein, we explore simultaneous doping of S and Ti^{3+} into TiO_2 nanotubes. We find that co-doped samples show considerable noble-metal-free photocatalytic H_2 evolution ability.

Results and Discussion

Figure 1 shows SEM images of TiO_2 nanotubes decorated with TiO_2 nanoparticles (here pristine means the sample without further H_2S annealing treatment, Fig. 1a) as well as after treatment in a mixture of 90% H_2/10% H_2S at 500°C for 30 minutes (H_2/H_2S-500-30, Fig. 1b). Throughout the manuscript we use an annotation of samples defined by atmosphere-temperature-time (minutes). A detailed description of sample preparation process can be found in the Experimental Section. Figure 1a shows that uniform TiO_2 nanoparticles with an average diameter of ca. 25 nm are formed that are well distributed on the inner and outer walls of the TiO_2 nanotubes. After annealing in H_2/H_2S, the TiO_2 particles at the top part of the nanotubes (TiO_2-H_2/H_2S-500-30) partially grow (Figure 1b) but the morphology of the TiO_2 nanotube scaffold remains. Considering that the radius of S^{2-} (184 pm) is larger than that of O^{2-} (132 pm), the size of particle should increase when a S^{2-} ion replaces an O^{2-} site. Such results can also be observed for particle decorated samples annealed in pure H_2S (TiO_2-H_2S-500-30) as shown in Figure S1d.

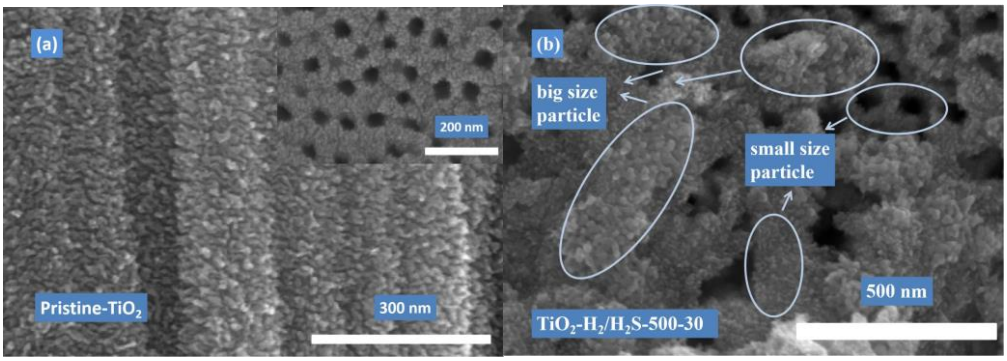

Figure 1. (a) SEM images of pristine TiO_2 nanotubes; (b) SEM images of TiO_2-H_2/H_2S-500-30.

Energy Dispersive X-ray Spectroscopy (EDS) was employed in order to determine the sulfur content of samples treated at 500 ºC under different gas atmospheres and for different durations (Table S1). The sulfur content of the sample increases with the annealing time in H_2/H_2S atmosphere. It rises from 0.33 at.% after annealing for 5 min to 0.84 at.% after annealing for 1 h. The bulk concentration of S is also higher when annealed in pure H_2S (1.74 at.%) than for annealing in H_2/H_2S (0.65 at.%) (both treated at 500 °C for 30 min) .

Figure 2a displays the photocatalytic hydrogen production results for a series of TiO_2-H_2/H_2S samples. The experiments were performed under open-circuit conditions and in the absence of any co-catalysts. The samples were directly immersed in an aqueous methanol solution (50 vol %) and illuminated under a 365 nm LED (140 mW/cm^2). The figure shows that the samples annealed in a gas mixture of H_2/H_2S overall evolve higher amounts of H_2 than pristine TiO_2. This is apparent already for samples treated in the gas mixture H_2/H_2S for only 2 minutes (TiO_2-H_2/H_2S-500-2). At an annealing temperature of 500°C, the H_2 evolution of samples first increases and then declines as a function of annealing time. The sample TiO_2-H_2/H_2S-500-30 shows the highest H_2 evolution rate of 22.3 $\mu L \cdot h^{-1} \cdot cm^{-2}$, which is almost 11 times higher than that of a pristine TiO_2 sample. For annealing temperatures higher than 500°C in H_2/H_2S

atmosphere, the TiO_2 nanotube layers started detaching from the Ti substrate. Samples annealed at lower temperature (450°C) are less active than samples annealed at 500 °C.

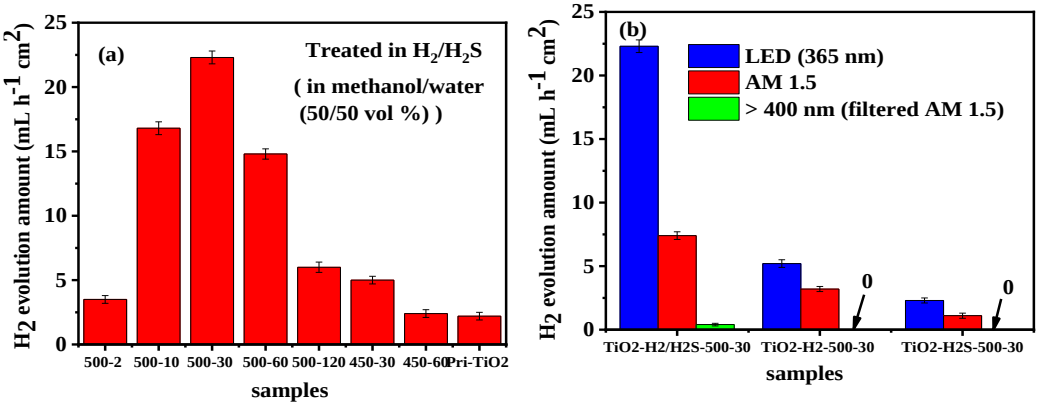

Figure 2. (a) Photocatalytic H_2 production of a series of TiO_2-H_2/H_2S samples under open circuit conditions under LED (365 nm, 140 mW/cm^2) illumination; (b) Photocatalytic H_2 production of TiO_2-H_2-500-30, TiO_2-H_2S-500-30 and TiO_2-H_2/H_2S-500-30 under LED, AM 1.5 (100 mW/cm^2) and AM 1.5 with a 400 nm filter illumination.

Therefore, in order to elucidate the effect of different atmospheres, reference samples were annealed in pure H_2 or H_2S under the optimized experimental conditions (at 500°C for 30 minutes). The photocatalytic H_2 production experiments were carried out under 365 nm LED illumination. To further check for an activity under visible light, the experiments were also performed under simulated solar light (AM 1.5, 100 mW/cm^2) and AM 1.5 with a 400 nm filter. The photo activity of samples treated in H_2/H_2S is much higher than those of reference samples under above illumination conditions. Under 365 nm LED irradiation, the H_2 production rate of TiO_2-H_2/H_2S-500-30 is 10 times higher than that of TiO_2-H_2S-500-30 and 4 times higher than that of TiO_2-H_2-500-30. Under AM 1.5 irradiation, the H_2 evolution rate of the optimized sample TiO_2-H_2/H_2S-500-30 is 7 times higher than that of TiO_2-H_2S-500-30. However, under AM 1.5 illumination with a 400 nm filter, the activity of all samples is almost completely lost.

The crystalline structures of pristine TiO_2, TiO_2-H_2-500-30, TiO_2-H_2S-500-30 and TiO_2-H_2/H_2S-500-30 were characterized by XRD (Figure 3). For all samples, typical diffraction peaks of anatase TiO_2 i.e. (101) at 25.2°, (004) at 38.4°, (200) at 48.0°, (105) at 53.9° and (211) at 55.1° (PDF card No. 00-021-1272) can be observed. Moreover, small peaks of rutile at 27.3°, 36.1° (PDF card No. 00-021-1276) and underlying Ti metal peaks at 35.1°, 38.4°, 40.1°, 52.9° (PDF card No. 00-044-1294) can also be identified. Neither sulfur crystal peaks (usually present at 23° for S_8 [25]) nor obvious peak shifts of anatase peaks in the sulfurized samples are observed.

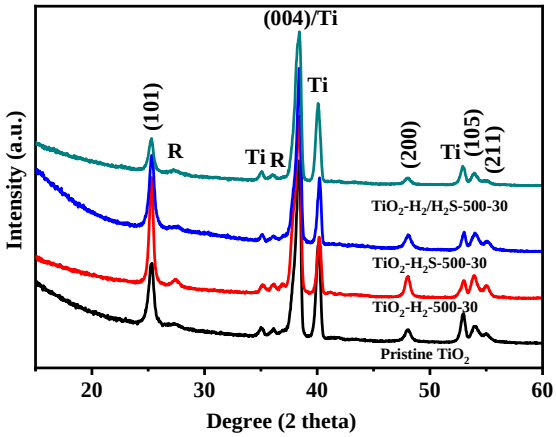

Figure.3. XRD patterns of pristine TiO_2, TiO_2-H_2-500-30, TiO_2-H_2S-500-30 and TiO_2-H_2/H_2S-500-30.

Nevertheless, successful chemical conversion from TiO_2 to TiS_2 or $TiO_{2-x}S_x$ by the H_2S treatment can be seen by X-ray Photoelectron Spectroscopy (XPS) (Figure 4). The sample treated in H_2S (TiO_2-H_2S-500-30) shows a broad S2p peak. The S2p peak can be deconvoluted into four components.[26-28] The sulfur peaks found in the range from 161 to 165 eV were deconvoluted into two pairs of S $2p_{3/2}$ and $2p_{1/2}$ peaks assigned to a O-Ti-S mixed state (with a binding energy between S-O and S-Ti). Additionally, S 2p peaks at binding energies around 168 eV can be separated into two peaks with binding energies of 167.5 and 168.7 eV, corresponding to S^{4+} and S^{6+} respectively.[26,27]

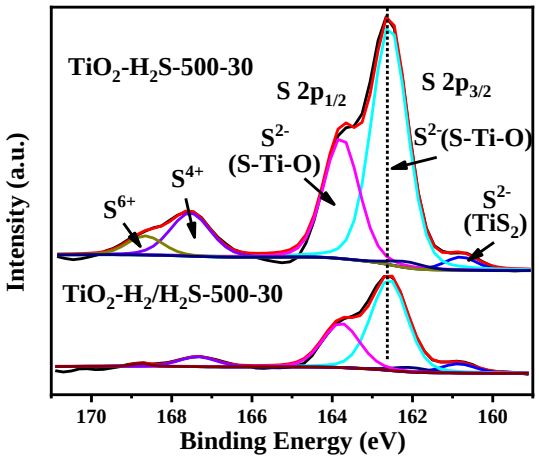

Figure.4. XPS S2p spectra of TiO_2-H_2S-500-30 and TiO_2-H_2/H_2S-500-30.

Zhang *et.al* reported that if sulfur was incorporated as S^{4+} into the crystal lattice of TiO_2, replacing Ti^{4+}, a peak at a binding energy of 167.5 eV can be found – this in contrast to SO_4^{2-} that is found at 168.8 eV. [28] Under our experimental conditions, the sulfur mainly exists in the form as S^{2-} and small amount of S^{4+}/S^{6+}. The shape and peak positions of S2p spectrum for TiO_2-H_2/H_2S-500-30 are similar to that of TiO_2-H_2S-500-30. The S content in TiO_2-H_2S-500-30 and TiO_2-H_2/H_2S-500-30 by XPS are 3.8 at.% and 2.3 at.% respectively, as shown in Table S2.

The presence of Ti^{3+} was investigated by electron paramagnetic resonance (EPR) spectroscopy. As shown in Figure 5a-d, TiO_2-H_2S-500-30 shows a high intensity of a resonance signal centered at the *g*-value of 1.99 with a high axial symmetry. Such Ti^{3+} states in anatase have been widely reported for Ti^{3+} ions in regular lattice positions.[29] For the TiO_2-H_2/H_2S-500-30 sample a very strong EPR signal at g=1.99 and a weak signal at g=1.94, is observed. For the hydrogenated sample, also a weak resonance signal of a broad width can be identified at g=1.94,[30-31] which can be attributed to Ti^{3+} dislocated from the regular position.[21] In line with literature, EPR signals at g=1.92-1.97 are observed in various TiO_2 structures annealed in Ar/H_2[29] or high pressure H_2.[20] Above results demonstrate that annealing in H_2/H_2S or H_2 creates Ti^{3+} defects (not shown for TiO_2 annealed in H_2S), which are responsible for hydrogen evolution under open circuit conditions.[21-22]

Incident photon-to-current conversion efficiency (IPCE) measurements of pristine TiO_2, TiO_2-H_2S-500-30 and TiO_2-H_2/H_2S-500-30 are shown in Figure 6a. In comparison with the reference samples, the TiO_2-H_2/H_2S-500-30 sample exhibits a greatly enhanced photocatalytic performance not only in the UV region but also in the visible light region. The IPCE at 330 nm of TiO_2-H_2/H_2S-500-30 reaches a value higher than 65%. Figure 6a (inset) presents the $(IPCE*h\nu)^{0.5}$ vs. $h\nu$ plots, from which the band gap (E_g) values can be evaluated (shown in Table 1).

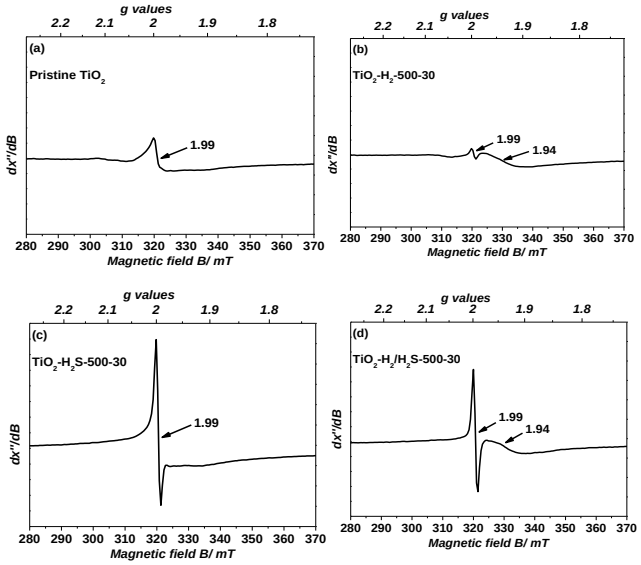

Figure.5. (a)-(d) EPR spectra of pristine TiO_2, TiO_2-H_2-500-30, TiO_2-H_2S-500-30 and TiO_2-H_2/H_2S-500-30.

Table.1. Band gap (E_g) of pristine TiO_2, TiO_2-H_2S-500-30 and TiO_2-H_2/H_2S-500-30 derived from IPCE plots.

samples	**Eg (eV)**
Pristine TiO_2	3.20
TiO_2-H_2/H_2S-500-30	3.11 2.0

TiO_2-H_2S-500-30	3.18	2.05

The band gap of pristine TiO_2 and of TiO_2-H_2S-500-30 is ≈ 3.20 eV, which corresponds to the characteristic value of anatase.[5] The primary E_g of the TiO_2-H_2/H_2S-500-30 sample is 3.11 eV, with a tail to 2.0 eV, which can be attributed to the S^{2-} and Ti^{3+} co-doping effect. These results reveal that the sulfur dopants produce visible light absorption states in the band gap of TiO_2, which can enhance the adsorption and conversion of visible light part and thus improve the overall hydrogen evolution efficiency when AM1.5 light source is used.

The valence band (VB) positions obtained from XPS are shown in Figure 6b. The VB edge of pristine TiO_2 is located at 1.99 eV below the Fermi energy. Since the optical band gap of TiO_2 is 3.2 eV from IPCE (Figure 6a), the conduction band (CB) would be located at -1.21 eV. The VB edge of TiO_2-H_2-500-30 is located at 1.97 eV, which is very similar to that of pristine TiO_2, indicating that the Ti^{3+} defects introduced by H_2 do not significantly alter the VB levels of TiO_2. However, the VB profiles of TiO_2-H_2S-500-30 and TiO_2-H_2/H_2S-500-30 show a notable difference: The main VB edge is located at 1.68 and 1.90 eV. This indicates that sulfur doping results in a VB shift. This is in line with ab initio band calculations, where mixing of S2p states (substitutional) with the valence band increases the width of the VB.[32-34]

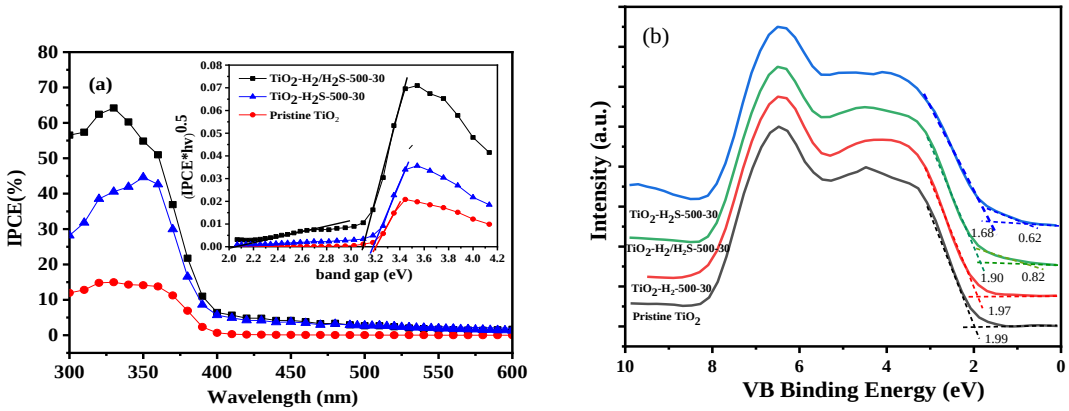

Figure.6. (a) IPCE spectra of pristine TiO_2, TiO_2-H_2S-500-30 and TiO_2-H_2/H_2S-500-30 in 0.1 M Na_2SO_4 (inset is evaluation of the band gap energy of the samples from IPCE plots); (b) VB XPS spectra of pristine TiO_2, TiO_2-H_2-500-30, TiO_2-H_2S-500-30 and TiO_2-H_2/H_2S-500-30.

Additionally, Mott-Schottky type of capacitance measurements were performed in order to obtain information on the flat band potential and carrier densities for different samples. According to the Mott-Schottky approach, the space charge capacitance (C_{SC}) of a semiconductor can be expressed as[35]

$$\frac{1}{C_{SC}^2} = \frac{2}{\varepsilon\varepsilon_0 q N_D}\left(E - E_{fb} - \frac{k_B T}{q}\right) \quad (1)$$

where C_{SC} is the space charge capacitance, E is the externally applied potential, E_{fb} is the flat band potential, N_D is the donor density, ε_0 is the permittivity of the free charge, ε is the permittivity of the semiconductor, q is the elementary charge, k_B is the Boltzmann constant and T is the temperature.

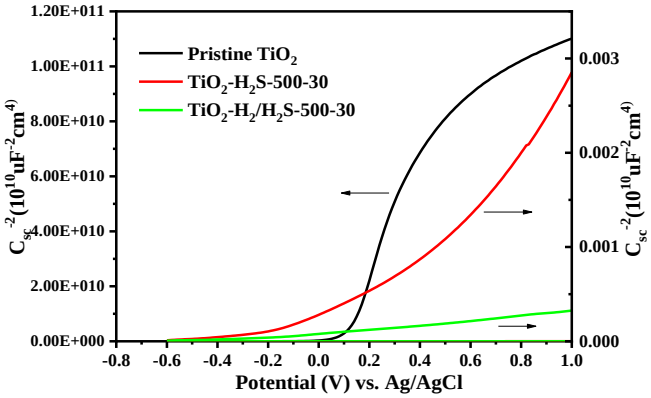

Figure.7. Mott-Schottky plots of pristine TiO_2, TiO_2-H_2S-500-30 and TiO_2-H_2/H_2S-500-30 in 0.1 M Na_2SO_4.

Figure 7 presents the M-S plots as $1/C^2$ vs. the applied potential. All samples show a positive slope in the M-S plots, as expected for an n-type semiconductor. The linear parts of the curves are extrapolated to $1/C^2=0$ according to eq. (1) and the values of E_{fb} are estimated to be 0.125, 0.055 and -0.33 V *vs.* Ag/AgCl for the pristine TiO_2, TiO_2-H_2S-500-30 and TiO_2-H_2/H_2S-500-30, respectively. The TiO_2-H_2/H_2S-500-30 shows the lowest flat band potential (E_{fb}). The negative shift of E_{fb} after reduction suggests a shift of the Fermi level as noted in XPS valence band measurements.

From the slopes of the MS measurements, the doping of densities can be established. As expected, the TiO_2-H_2/H_2S-500-30 present the highest carrier density (6.95×10^{23} cm^{-3}), followed by TiO_2-H_2S-500-30 (7.88×10^{22} cm^{-3}) and pristine TiO_2 (7.88×10^{18} cm^{-3}).

Furthermore, Figure 8a shows the photo-generated electron transfer time constants of samples obtained from intensity modulated photocurrent spectroscopy measurements (IMPS). From the results, the transport of electrons in TiO_2-H_2/H_2S-500-30 and TiO_2-H_2S-500-30 are faster than in pristine TiO_2. In comparison with TiO_2-H_2S-500-30, also TiO_2-H_2/H_2S-500-30 shows an evidently shorter transport time, which means the energetic structure of TiO_2-H_2/H_2S-500-30 can facilitate the migration of electrons.

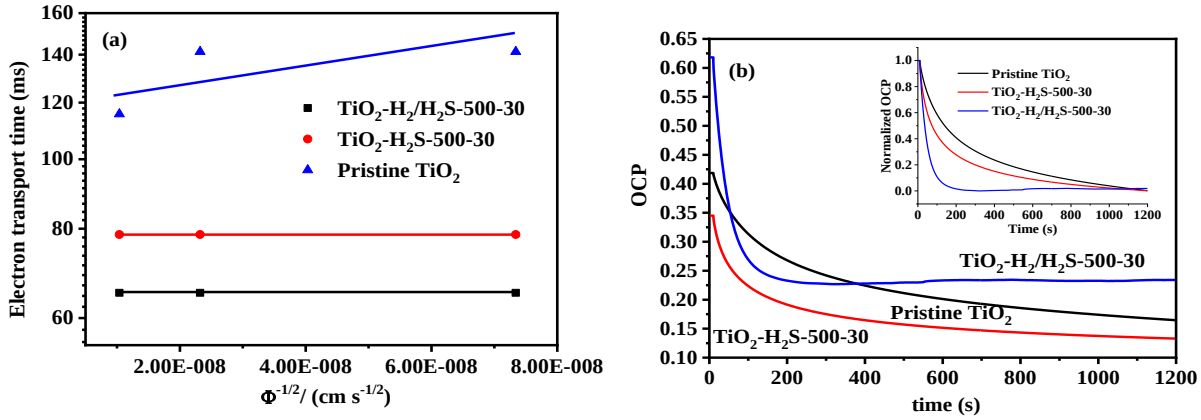

Figure.8. (a) IMPS spectra of pristine TiO_2, TiO_2-H_2S-500-30 and TiO_2-H_2/H_2S-500-30 in 0.1 M Na_2SO_4; (b) OCP of pristine TiO_2, TiO_2-H_2S-500-30 and TiO_2-H_2/H_2S-500-30 in 0.1 M Na_2SO_4.

Open circuit potential (OCP) decay measurements were carried out to estimate the photogenerated electron life times of samples as shown in Figure 8b. Pristine TiO_2 shows the lowest OCP value and TiO_2-H_2/H_2S-500-30 has the highest value, hence the number of free electrons that can migrate to the surface is the highest for TiO_2-H_2/H_2S-500-30. EPR results for TiO_2-H_2S-500-30 also show a strong Ti^{3+} signal at g=1.99, but such Ti^{3+} is not responsible for the acceleration of the transport of electrons or for the improvement of the photocatalytic activity.[29] However, the presence of a small amount of Ti^{3+} at g=1.94 is a signature of charge-transfer facilitating states.[21] For the sample TiO_2-H_2/H_2S-500-30 sulfur doping creates inter band-gap states which may additionally contribute to enhance the photocatalytic activity.

Based on the above results, we obtain the energy-level diagram of pristine TiO_2, TiO_2-H_2S-500-30 and TiO_2-H_2/H_2S-500-30, as depicted in Scheme 1.

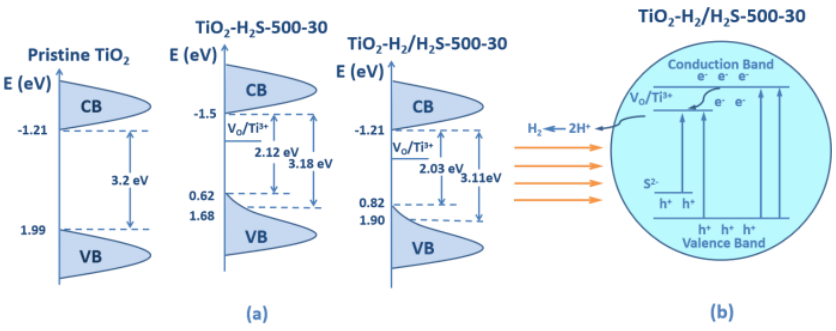

Scheme 1. (a) Schematic diagram of energy structures of pristine TiO_2, TiO_2-H_2S-500-30 and TiO_2-H_2/H_2S-500-30. (b) The photocatalytic H_2 evolution process in TiO_2-H_2/H_2S-500-30 under irradiation.

After sulfur and Ti^{3+} co-doping, the band gap of TiO_2-H_2/H_2S-500-30 shows a new absorption band in visible light region which is considered to be introduced by S2p, i.e., a new mid-gap state. The new band of 2.03 eV for TiO_2-H_2/H_2S-500-30 by calculation from the value of XPS VB measurements is very close to the result of the IPCE data (2.0 eV), likewise for TiO_2-H_2S-500-30.

Conclusions

In summary, sulfur and Ti^{3+} co-doped TiO_2 nanotubes were successfully prepared by annealing TiO_2 nanotubes in a H_2/H_2S gas mixture. The photocatalytic activity of H_2 evolution under UV light was enhanced for co-doped samples TiO_2-H_2/H_2S-500-30. It is concluded that the improved photo harvesting ability is not the key for the enhancement of photocatalytic performance. Instead, it is proposed that the increased activity can be mainly attributed to the synergetic effect of existence of both S mid-gap states and dislocated Ti^{3+} defects ($g \approx 1.93$), which can co-contribute to the photocatalytic activity of TiO_2-H_2/H_2S-500-30 photocatalyst. Co-doping with S and Ti^{3+} can not only modify the electronic structure but also may facilitate an efficient separation and restrain recombination of photo-generated electrons and holes to a large extent. It is confirmed that the number of photo-generated electrons to participate in the photocatalytic reaction increases in TiO_2-H_2/H_2S-500-30. The presented results expand the comprehensive understanding of the photo induced charge transfer in TiO_2 and provide a novel tool for TiO_2 applications in solar energy conversion.

Experimental Section

Preparation and modification of TiO_2 nanotube samples

For our experiments we used self-organized TiO_2 nanotube layers (NTs) grown from titanium metal sheets by electrochemical anodization process. Before anodization, the Ti foils (0.125 nm thickness, Advent, 99.6% high-purity) were sonicated in acetone, ethanol and deionized water for 15 min respectively, and then were dried in nitrogen stream. The TiO_2 NTs were formed by anodizing 1.5 x 1.5 cm Ti foil in a two-electrode configuration using platinum as a counter electrode at 60 V for 50 min. The electrolyte consisted of 0.2 M NH_4F (98%, Sigma-Aldrich), 1 M DI water and ethylene glycol (99.5%, Sigma-Aldrich). The anodized samples were rinsed by ethanol directly to remove residual electrolyte and then immersed in ethanol overnight. In order to convert the amorphous as-anodized TiO_2 tubes to crystalline tubes, thermal annealing was performed in air at 450 °C for 3 hours. In order to increase the surface area of the NT layers, the TiO_2 NTs were surface modified by decorating with TiO_2 nanoparticles through treatment in $TiCl_4$ solution. For this, the crystallized TiO_2 NTs were immersed in 0.2 M aqueous solutions of $TiCl_4$ prepared under ice-cooled conditions, and kept them at 70 °C for 30 min in order to form nanoparticles on the tubes during the second growth process. The reactions between $TiCl_4$ and H_2O are as follows:

$$TiCl_4 + XH_2O – Ti(OH)_xCl_{4-x} + xHCl \quad (1)$$

$$Ti(OH)_xCl_{4-x} – TiO_2 + (4-x)HCl + (X-2)H_2O \quad (2)$$

Afterwards, all treated samples were washed with water and ethanol and then dried in nitrogen stream. After the $TiCl_4$ treatment, samples were annealed again at 450 °C for 30 min to crystallize the attached TiO_2 nanoparticles. The TiO_2 nanotubes with nanoparticles were marked as pristine TiO_2 for reference.

The as-prepared samples were annealed in a gas mixture of H_2/H_2S (90%/10%) at different conditions. For reference, samples were also annealed in pure H_2 or pure H_2S.

Characterization

In order to characterize the morphology of the samples, a field-emission scanning electron microscope (SEM, Hitachi S4800) was used. An X-ray photoelectron spectrometer (XPS, PHI 5600 XPS spectrometer) was used to obtain information on the chemical composition of the samples; all XPS element peaks were shifted in relation to C standard position. XRD patterns of the crystallized TiO_2 NTs were collected using an X-ray diffractometer (X\pert Philips PMD diffractometer) equipped with a Panalytical X\celerator detector and using graphite monochromized CuKα radiation (λ=1.54056 Å). The photoluminescence (PL) spectra were measured at room temperature on a fluorescence spectrometer (iHR320 monochromator and Synergy Si CCD camera (both Horiba Jobin-Yvon)) with an excitation wavelength of 325 nm diode laser at room temperature.

EPR spectra were recorded on a JEOL continuous wave spectrometer JES-FA200 equipped with an X-band Gunn oscillator bridge, a cylindrical mode cavity, and a helium cryostat. The samples were measured in the solid state in an air atmosphere in quartz EPR tubes with comparable loading. Background spectra were obtained on empty tubes at the same measurement conditions. The spectra shown were measured with the following parameters: Tempearture 77 K, microwave frequency 8.963 GHz, modulation width 2.0 mT, microwave power 1.0 mW, modulation frequency 100 kHz, and time constant 0.1 s.

Mott-Schottky measurements were performed on a Zahner IM6 (Zahner Elektrik, Kronach, Germany) work station under dark conditions in 0.1 M Na_2SO_4. A three-electrode cell with Pt as a counter electrode, the sample as a working electrode and Ag/AgCl (saturated KCl) as a reference electrode was used. The potential window applied was -0.6 V to 1.0 V and the capacitance data was evaluated at 1 Hz.

Intensity modulated photocurrent spectroscopy (IMPS) measurements were carried out with modulated light (10% modulation depth) from UV light emitting diode (λ=369 nm). The modulation frequency was controlled by a frequency response analyzer (FRA, Zahner IM6, Kronach, Germany) and the photocurrent or photovoltage of cell was recorded by an electrochemical interface (Zahner IM6), and then fed back to FRA. The light intensity incident on the cell was measured using a calibrated Si photodiode. A three-electrode cell with Pt as a counter electrode, a Haber-Luggin capillary with Ag/AgCl (saturated KCl) electrode as a reference electrode and the sample as a working electrode was used. The corresponding electron transport time constants were evaluated by IMPS. The technique exhibits a specific frequency f_{IMPS} which is inversely proportional to electron transport time (t_{tr}) according to Eq. (3):

$$t_{tr} = \frac{1}{2\pi f_{IMPS}} \qquad (3)$$

The open-circuit potential (OCP) decay characterizations were also carried out by irradiating sample for 10 s and then recording the voltage generated by photo induced electrons as a function of time.

The incident photon to current conversion efficiency (IPCE) measurements were carried out with a setup consisting of a 150 W Xe arc lamp (LOT-Oriel Instruments) as the irradiation source and a Cornerstone motorized 1/8 m monochromator. Photocurrent spectra were acquired in 0.1 M (Na_2SO_4) at a potential of 500 mV (vs. Ag/AgCl). Photocurrent spectra were measured in a three-electrode conFigureuration, consisting of TiO_2 nanotubes as photoanode, platinum foil as a counter electrode and an Ag/AgCl electrode as a reference by a JAISSLE IMP 83 PCT-BC Poentiostat-Galvanostat. The electrochemical cell was adjusted horizontally in front of the light source. IPCE for each wavelength was calculated according to Eq. (4):

$$\mathrm{IPCE} = \frac{(1240\mathrm{I})}{\lambda\, \mathrm{J_{light}}} \qquad (4)$$

where I is the measured photocurrent density at a specific wavelength, λ is the wavelength of incident light, and J_{light} is the measured power density at a specific wavelength.

Measurement of photocatalytic activities

The photocatalytic activities of the samples were evaluated by H_2 evolution measurements under open-circuit condition without co-catalyst. The TiO_2 NTs were immersed in an aqueous methanol solution (50 vol.%) and illuminated by led light (365 nm, 140 mW/cm^2) or an AM 1.5 solar simulator (100 mW/cm^2). A gas chromatography (GCMS-QO2010SE, SHIMADZU) with TCD detector was used to obtain the amount of H_2 generated from the different TiO_2 NTs samples.

Acknowledgements

We thank Prof. Dr. Karsten Meyer and Dominik Fehn for EPR measurements and helpful discussions. Financial support from ERC and DFG within the framework of its Excellence Initiative for the Cluster of Excellence "Engineering of Advanced Materials" is thankfully acknowledged. The author would also like to thank the Chinese Scholarship Council for financial support for Prof. Ji's visit to department of Materials Science, WW-4, University of Erlangen-Nuremberg.

References

[1] A. Fujishima and K. Honda, *Nature*, **1972**, *238*, 37-38.

[2] M. R. Hoffmann, S. T. Martin, W. Choi, and D. W. Bahnemann, *Chem. Rev.*, **1995**, *95*, 69-96.

[3] X. Chen, S. Shen, L. Guo, and S. S. Mao, *Chem. Rev.*, **2010**, *110*, 6503-6570.

[4] T. Hisatomi, J. Kubota, and K. Domen, *Chem. Soc. Rev.*, **2014**, *43*, 7520-7535.

[5] X. Chen and S. S. Mao, *Chem. Rev.*, **2007**, *107*, 2891-2959.

[6] C.-H. Liao, C.-W. Huang, and J. C. S. Wu, *Catalysts*, **2012**, *2*, 490-516.

[7] A. Fujishima, T. N. Rao, and D. A. Tryk, *J. Photochem. Photobiol. C Photochem. Rev.*, **2000**, *1*, 1-21.

[8] H. Tong, S. Ouyang, Y. Bi, N. Umezawa, M. Oshikiri, and J. Ye, *Adv. Mater.*, **2012**, *24*, 229-251.

[9] S. U. M. Khan, *Science*, **2002**, *297*, 2243-2245.

[10] X. Chen and C. Burda, *J. Am. Chem. Soc.*, **2008**, *130*, 5018-5019.

[11] W. Ho, J. C. Yu, and S. Lee, *J. Solid State Chem.*, **2006**, *179*, 1171–1176.

[12] P. Periyat, S. C. Pillai, D. E. McCormack, J. Colreavy, and S. J. Hinder, *J. Phys. Chem. C*, **2008**, *112*, 7644-7652.

[13] T. Ohno, T. Mitsui, and M. Matsumura, *Chem. Lett.*, **2003**, *32*, 364-365.

[14] M. R. Bayati, A. Z. Moshfegh, and F. Golestani-Fard, *Appl. Catal. A Gen.*, **2010**, *389*, 60-67.

[15] S. W. Shin, J. Y. Lee, K.-S. Ahn, S. H. Kang, and J. H. Kim, *J. Phys. Chem. C*, **2015**, *119*, 13375-13383.

[16] X. Tang, D. Li, and A. Tg, *J. Phys. Chem. C*, **2008**, *112*, 5405–5409.

[17] X. Pan, M.-Q. Yang, X. Fu, N. Zhang, and Y.-J. Xu, *Nanoscale*, **2013**, *5*, 3601-3614.

[18] N. Liu, N. Liu, V. Häublein, X. Zhou, U. Venkatesan, M. Hartmann, M. Mačković, T. Nakajima, E. Spiecker, A. Osvet, L. Frey, and P. Schmuki, *Nano Lett.*, **2015**, *15*, 6815-6820.

[19] X. Chen, L. Liu, P. Y. Yu, and S. S. Mao, *Science*, **2011**, *331*, 746-750.

[20] N. Liu, C. Schneider, D. Freitag, M. Hartmann, U. Venkatesan, J. Müller, E. Spiecker, and P. Schmuki, *Nano Lett.*, **2014**, *14*, 3309-3313.

[21] X. Zhou, N. Liu, J. Schmidt, A. Kahnt, A. Osvet, S. Romeis, E. M. Zolnhofer, V. R. R. Marthala, D. M. Guldi, W. Peukert, M. Hartmann, K. Meyer, and P. Schmuki, *Adv. Mater.*, **2017**, *29*, 1604747.

[22] N. Liu, N. Liu, C. Schneider, D. Freitag, U. Venkatesan, V. R. R. Marthala, M. Hartmann, B. Winter, E. Spiecker, A. Osvet, E. M. Zolnhofer, K. Meyer, T. Nakajima, X. Zhou, and P. Schmuki, *Angew. Chem. Int. Ed.*, **2014**, *53*, 14201-14205.

[23] A. Naldoni, M. Altomare, G. Zoppellaro, N. Liu, Š. Kment, R. Zbořil, and P. Schmuki, *ACS Catal.*, **2019**, *9*, 345-364.

[24] X. Zhou, N. Liu, and P. Schmuki, *ACS Catal.*, **2017**, *7*, 3210-3235.

[25] G. Liu, P. Niu, L. Yin, and H. Cheng, *J. Am. Chem. Soc.*, **2012**, *134*, 9070-9073.

[26] M. R. Bayati, A. Z. Moshfegh, and F. Golestani-Fard, *Appl. Catal. A Gen.*, **2010**, *389*, 60-67.

[27] S. Sun, J. Zhang, P. Gao, Y. Wang, X. Li, T. Wu, Y. Wang, Y. Chen, P. Yang, *Appl. Catal. B Environ.*, **2017**, *206*, 168-174.

[28] Y. Niu, M. Xing, B. Tian, and J. Zhang, *Appl. Catal. B Environ.*, **2012**, *115-116*, 253-260.

[29] S. Mohajernia, S. Hejazi, A. Mazare, N. T. Nguyen, and P. Schmuki, *Chem. -A Eur. J.*, **2017**, *23*, 12406-12411.

[30] J. C. Conesa and J. Soria, *J. Phys. Chem.*, **1982**, *86*, 1392-1395.

[31] M. Xing, J. Zhang, F. Chen, and B. Tian, *Chem. Commun.*, **2011**, *47*, 4947-4949.

[32] T. Umebayashi, T. Yamaki, S. Yamamoto, A. Miyashita, S. Tanaka, T. Sumita, and K. Asai, *J. Appl. Phys.*, **2003**, *93*, 5156-5160.

[33] T. Umebayashi, T. Yamaki, H. Itoh, and K. Asai, *Appl. Phys. Lett.*, **2002**, *81*, 454-456.

[34] T. Yamamoto, F. Yamashita, I. Tanaka, E. Matsubara, and A. Muramatsu, *Mater. Trans.*, **2004**, *45*, 1987-1990.

[35] H. Tsuchiya, J. M. Macak, A. Ghicov, A. S. Räder, L. Taveira, and P. Schmuki, *Corros. Sci.*, **2007**, *49*, 203-210.